In situ determination of aging precipitation in deformed Fe-Cu and Fe-Cu-B-N alloys by time-resolved small-angle neutron scattering

S. M. He,[1,*] N. H. van Dijk,[1] M. Paladugu,[1] H. Schut,[2] J. Kohlbrecher,[3] F. D. Tichelaar,[4] and S. van der Zwaag[5]

[1]*Fundamental Aspects of Materials and Energy, Faculty of Applied Sciences, Delft University of Technology, Mekelweg 15, 2629 JB Delft, The Netherlands*

[2]*Neutron and Positron Methods in Materials, Faculty of Applied Sciences, Delft University of Technology, Mekelweg 15, 2629 JB Delft, The Netherlands*

[3]*Laboratory for Neutron Scattering, ETHZ and PSI, CH-5232 Villigen PSI, Switzerland*

[4]*Kavli Institute of Nanoscience, National Centre for HREM, Delft University of Technology, Lorentzweg 1, 2628 CJ Delft, The Netherlands*

[5]*Novel Aerospace Materials, Faculty of Aerospace Engineering, Kluyverweg 1, 2629 HS Delft, The Netherlands*

We performed *in situ* time-resolved small-angle neutron scattering (SANS) measurements on high-purity Fe-Cu and Fe-Cu-B-N alloys during isothermal aging at 550 °C in order to study the potential self-healing of deformation-induced defects by nanosized Cu precipitation. Three different samples with 0%, 8%, and 24% prestrain were used to study the influence of variable defect levels on the Cu precipitation kinetics. The time-resolved SANS measurements show the presence of two contributions corresponding to spherical precipitates and precipitation at dislocations and/or interfaces, as confirmed by complementary transmission electron microscopy experiments. For the Fe-Cu alloy, prestrain was found to accelerate the formation of spherical precipitates in initial aging stage and lead to a significant enhancement of copper precipitation at dislocations and/or interfaces. For the Fe-Cu-B-N alloy, the addition of boron and nitrogen accelerates the formation of spherical precipitates but suppresses the precipitation along dislocations in the prestrained samples.

I. INTRODUCTION

Steels are among the most widely used construction materials as their mechanical properties can be tailored to obtain the required combination of strength and formability. However, in highly demanding applications the lifetime until failure of steels is limited due to the accumulation of damage, ultimately leading to the formation of ultrafine cracks that subsequently grow and ultimately cause fracture of the steel components.

Recently it was recognized that in aluminum alloys[1] and steels[2,3] the growth of ultrafine cracks can be immobilized in an early stage by the dynamic formation of nanoscale precipitates. This process is known as self-healing and can significantly enhance the lifetime of structural components. So far, relatively little research has been done on self-healing in metals.[4] For austenitic stainless steels,[2,3] dynamic precipitation of both Cu and BN was found to reduce creep damage under a load at high temperatures. The precipitates are assumed to partly fill the nanoscale open volume defects and thereby prevent their further growth.

In order to fully understand the role of these alloying elements and the influence of thermomechanical processing on the defect-induced precipitation, responsible for self-healing, additional studies on less complex low-alloyed steel grades are desirable. Therefore, high-purity Fe-Cu and Fe-Cu-B-N model alloys have been prepared in order to identify the physical mechanism responsible for self-healing in ferritic steels [with a body-centered-cubic (bcc) matrix]. This insight will then make it possible to successfully introduce these concepts in industrial steel grades.

The precipitation of copper from supersaturated Fe-Cu alloys has been investigated extensively, both

experimentally[5–20] and theoretically.[21–24] It is now generally accepted that, in the initial stage, fully coherent Cu precipitates inherit the bcc structure of the α-Fe matrix. When reaching a critical diameter of approximately 4–6 nm, the growing bcc precipitates undergo a martensitic transformation to a less coherent 9R structure. At sizes larger than 15–17 nm, a second transformation to the more stable 3R structure takes place before the Cu precipitates adopt their equilibrium face-centered-cubic (fcc) structure. The full transformation sequence for copper precipitation in Fe-Cu alloys is given by bcc$\rightarrow$9R$\rightarrow$3R$\rightarrow$fcc for increasing aging time. As far as the composition of Cu precipitates is concerned, the Cu precipitates are almost pure Cu at sizes above 4–5 nm but there exists contradicting information about their composition during the initial stage of the precipitation process. Investigations performed with atom probe analysis consistently report that the early Cu precipitates contain a significant fraction of Fe (in some cases even in excess of 50 at. %),[9–12] which was later supported by thermodynamic calculations.[24] The probe analysis, nevertheless, can generate a large statistical error and underestimate the solute concentration in small precipitates due to the finite probe resolution. In contrast, results obtained with small-angle neutron scattering (SANS) (Refs. 13–16) and positron annihilation[17–20] suggest that the precipitates are almost pure Cu with only minor amounts of Fe. Interpretation of the latter experiments depends however on *a priori* knowledge of the physical properties of the small Cu clusters, which may cause some uncertainty in the determination of the composition of the Cu precipitates in the initial stage of the precipitation process. The composition of the metastable ultrafine bcc Cu precipitates in the Fe-Cu system is therefore still an open question.

TABLE I. Chemical composition of the studied high-purity model alloys (in wt %) with balance iron. The Ce content refers to the added nominal composition.

Alloy	Cu	B	N	C	S	Ce
Fe-Cu	1.11	<0.01	0.002	0.0056	0.002	0.015
Fe-Cu-B-N	1.06	0.052	0.029	0.0032	0.002	0.015

More theoretical and experimental investigations are needed to solve this controversy.

In order to unravel the mechanism responsible for self-healing in steels it is essential to obtain detailed information on (i) the influence of open-volume defects (vacancies, vacancy clusters, and dislocations) and (ii) microalloying with B and N on the Cu precipitation kinetics in Fe-Cu alloys, which is currently not available. It is well known that open-volume defects facilitate the diffusion of solutes and thereby accelerate the precipitation, which is expected to promote the self-healing of metals by dynamic precipitation. Dislocations, which are easily multiplied by deformation, are found to accelerate the diffusion of impurities by almost three orders of magnitude compared to bulk diffusion[25] and have been proposed to play a role as heterogeneous nucleation sites for Cu precipitation.[26] The addition of boron and nitrogen was found to suppress creep cavity growth in copper-containing stainless steels, leading to a higher rupture strength and rupture ductility.[3] The effect of boron and nitrogen on the copper precipitation mechanism has so far not been clarified.

Although the Cu precipitation kinetics of Fe-Cu has been investigated in earlier SANS (Refs. [13]–[16] and [27]) and small-angle x-ray scattering (SAXS) experiments,[28,29] limited information is available on the precipitation behavior before peak aging. Previous SANS and SAXS experiments were all performed *ex situ* (at room temperature) and neither concentrate on the effect of deformation on the Cu precipitation nor on the addition of B and N.

In order to establish the potential of self-healing of defects by dynamic precipitation and to reach a detailed understanding of the influence of both deformation and added boron and nitrogen on the Cu precipitation in iron-based alloys, we performed *in situ* time-resolved SANS measurements on predeformed high-purity Fe-Cu and Fe-Cu-B-N alloys during isothermal aging at high temperatures. These time-resolved SANS measurements provide valuable information on the evolution of the precipitate size distribution. For comparison, complementary hardness tests and transmission electron microscope (TEM) observations have been performed. The results are compared to earlier positron annihilation spectroscopy measurements[30] performed on the same alloys.

II. EXPERIMENTAL METHODS

A. Material, heat treatments, and hardness tests

The chemical composition of the studied high-purity Fe-Cu and Fe-Cu-B-N alloys is listed in Table I. Both alloys

were produced by Goodfellow as a rolled sheet with a thickness of 0.5 mm. From this material dog-bone (I) shaped samples were cut by spark erosion for tensile deformation tests. The samples were solution treated at 850 °C for 1 h in evacuated silica tubes filled with 200 mbar ultrahigh-purity argon gas and subsequently quenched into water at room temperature. This solution treatment resulted in a fully equiaxed ferritic structure with a grain size of approximately 60 μm. Part of the as-quenched samples were subjected to tensile deformation at room temperature up to a strain of 8% or 24% using a 2 kN microtensile tester (Deben) with an initial slow strain rate of 2.67×10^{-4} s^{-1}.

Hardness test were performed on samples that were aged for 0–100 h at 550 °C in a salt bath. For the hardness tests a Buehler microhardness tester was used with a Vickers microhardness indenter, a load of 4.9 N and a holding time of 15 s.

B. Small-angle neutron scattering

In order to study the self-healing mechanism of defects by the formation of nanosized Cu precipitates and the role of added boron and nitrogen in copper-based iron alloys, time-resolved SANS measurements on the Fe-Cu and Fe-Cu-B-N alloys were carried out on the instrument SANS-I at PSI, Switzerland. These experiments were performed on the alloy samples during 12 h of aging at a constant temperature of 550 °C in a vacuum chamber ($<10^{-2}$ Pa) to monitor the precipitation kinetics of Cu precipitates in: (a) undeformed and plastically predeformed samples with (b) 8% and (c) 24% strain. The applied heating rate at the start of the experiments was of 73 °C/min (1.2 °C/s). The *in situ* SANS measurements were performed with a neutron wavelength of $\lambda = 0.7$ nm ($\Delta\lambda/\lambda = 10\%$) at sample-to-detector distances of 2, 6, and 18 m (longest distance was only used before and after aging). During aging at 550 °C time-resolved measurements SANS were performed by continuously switching the sample-to-detector distance between 2 and 6 m. The exposure time at each position was 150 s for the first hour and 300 s afterward. A transverse magnetic field of 1.1 T was applied perpendicular to the incident neutron beam in order to separate the nuclear (isotropic) and magnetic (anisotropic) scattering.

C. Transmission electron microscopy

Disks for transmission electron microscopy were prepared by mechanical grinding down to 80 μm. The thin foils were then etched in a Tenupol jet polisher with a 5% perchloric acid—95% acetic acid solution, held at 15 °C using a voltage of 35 V. Microscopy was carried out using a Philips CM30T operating at 300 kV and a Tecnai F20STEM/ST operating at 200 kV. Image analysis was conducted on two samples with 0% and 8% prestrain which have been measured by SANS at 550 °C for 12 h.

III. RESULTS

A. Aging curves

In Fig. 1, the effect of aging at 550 °C on the hardness is shown for the as-quenched Fe-Cu and Fe-Cu-B-N alloys
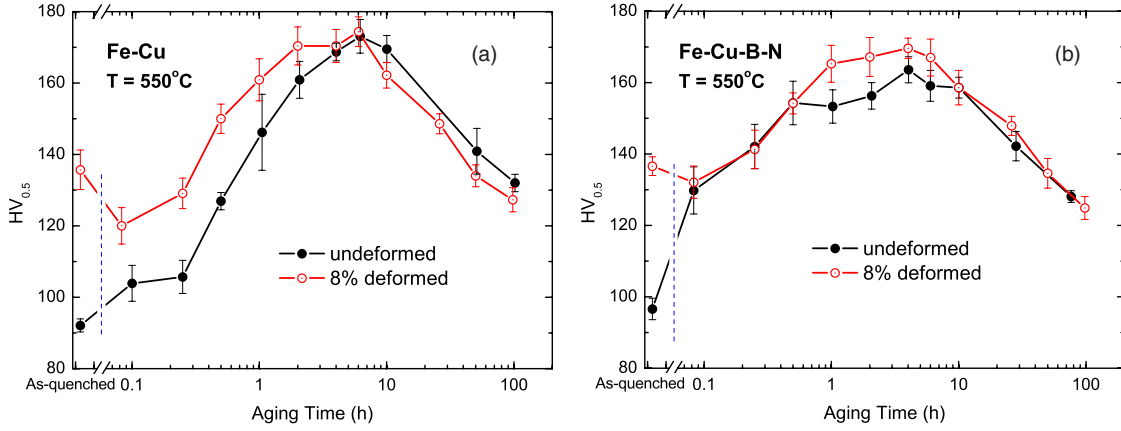
FIG. 1. (Color online) Hardness aging curves of the as-quenched Fe-Cu and Fe-Cu-B-N samples aged at 550 °C with and without 8% predeformation.

with and without 8% prestrain. For the undeformed alloys, the typical age-hardening behavior for copper precipitation is observed. The peak hardness is reached at about 6 h for the Fe-Cu alloy and 4 h for the Fe-Cu-B-N alloy. The 8% prestrain leads to a significant increase in the initial hardness caused by cold-work hardening, which reduces during aging. The hardness of the deformed alloys with 8% prestrain decreases in the initial aging stage due to the recovery of dislocations, then rises quickly with aging in the regime from underaged to peak-aged, and finally decreases again in the overaged stage. For the Fe-Cu alloy, the hardness of the deformed sample exceeds that of the undeformed sample until the peak-aged regime is reached but seems to be lower than that of the undeformed sample in the overaged regime. For the Fe-Cu-B-N alloy, the hardness of the deformed sample is above that of undeformed sample in the peak-aged regime while the hardness of the deformed and undeformed samples is quite comparable in the underaged and overaged regime.

A comparison of the aging behavior of both alloys in Fig. 1 indicates that the Fe-Cu-B-N alloy has a faster response than the Fe-Cu alloy. This means that the precipitation of Fe-Cu alloy is accelerated by the addition of B and N. The time to peak hardness was found to be relatively insensitive to the predeformation: only for the Fe-Cu alloy the predeformation seems to result in a minor reduction in the time to peak hardness.

The results for the Fe-Cu alloy with 1.1 wt % Cu are in good agreement with earlier hardness studies on binary Fe-Cu alloys. Both the peak hardness and the aging time to peak are in between those reported for 0.8 wt % Cu (Ref. 28) and for 1.3 wt % Cu.[14] The observed effect of prestrain on the hardness during aging is consistent with that observed by Deschamps and co-workers.[28]

B. Small-angle neutron scattering

By applying a transverse magnetic field of $\mu_0 H = 1.1$ T, the magnetization of the ferromagnetic Fe-Cu alloy containing nonmagnetic Cu clusters (fcc copper is weakly diamagnetic) is nearly saturated with the spins in the ferromagnetic matrix aligned along the magnetic field (x axis) perpendicu-

lar to the incident neutron beam (z axis). Figure 2 shows the two-dimensional SANS patterns obtained for our Fe-Cu alloy with 24% prestrain before and after isothermal aging for 12 h at 550 °C. The data were recorded for a neutron wavelength of 7 Å at a sample-detector distance of 6 m. As shown in Fig. 2(a), a weakly anisotropic scattering pattern is observed before aging with a dominant scattering contribution perpendicular to the applied magnetic field. This anisotropy of the scattered intensity becomes more pronounced with increasing aging times. As shown in Fig. 2(b), a strongly anisotropic scattering pattern has formed after 12 h aging at 550 °C. From the two-dimensional patterns the SANS cross section $(\frac{d\Sigma}{d\Omega})(\mathbf{Q})$ can be obtained, where $\mathbf{Q} = (Q_x, Q_y, 0)$ is the scattering vector with a wave-vector transfer Q_x and Q_y along the horizontal (x) and vertical (y) axis, respectively. For a magnetically saturated sample the total SANS cross section can be expressed as a sum of both magnetic and nuclear scattering components,[31]

$$\left(\frac{d\Sigma}{d\Omega}\right) = \left(\frac{d\Sigma}{d\Omega}\right)_{\text{NUC}} + \left(\frac{d\Sigma}{d\Omega}\right)_{\text{MAG}} \sin^2 \alpha, \tag{1}$$

where α is the angle between applied magnetic field $\mathbf{H}$ (orientation of the magnetization of the specimen $\mathbf{M}$) and the scattering vector $\mathbf{Q}$. The scattered intensity along ($\alpha=0°$) and perpendicular ($\alpha=90°$) to the applied magnetic field is expressed as $(d\Sigma/d\Omega)_{\mathbf{H}\|\mathbf{Q}}$ and $(d\Sigma/d\Omega)_{\mathbf{H}\perp\mathbf{Q}}$, respectively. The nuclear (isotropic) and magnetic (anisotropic) scattering components correspond to

$$\left(\frac{d\Sigma}{d\Omega}\right)_{\text{NUC}} = \left(\frac{d\Sigma}{d\Omega}\right)_{\mathbf{H}\|\mathbf{Q}}, \tag{2}$$

$$\left(\frac{d\Sigma}{d\Omega}\right)_{\text{MAG}} = \left(\frac{d\Sigma}{d\Omega}\right)_{\mathbf{H}\perp\mathbf{Q}} - \left(\frac{d\Sigma}{d\Omega}\right)_{\mathbf{H}\|\mathbf{Q}}. \tag{3}$$

Since the complete two-dimensional scattering pattern is measured, the magnetic and nuclear scattering components can be obtained simultaneously from a fit of the full scattering pattern with Eq. (1). Figures 3 and 4 show the Q dependence of the nuclear (isotropic) and magnetic (anisotropic) scattering components for the Fe-Cu and Fe-Cu-B-N alloys
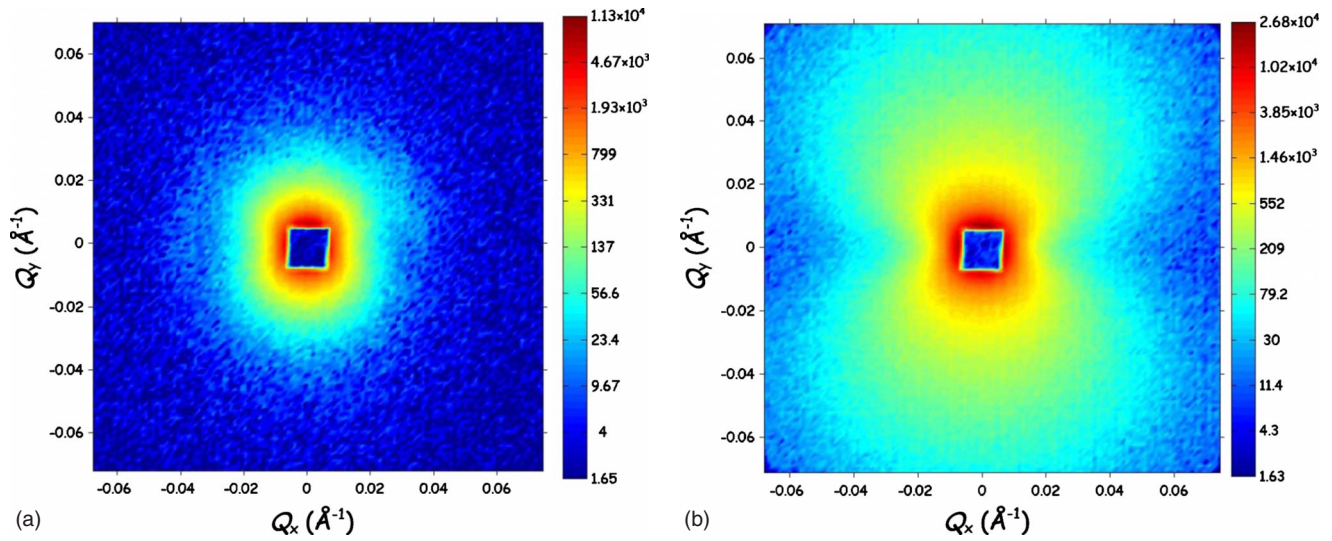
FIG. 2. (Color online) Small-angle neutron-scattering patterns of the Fe-Cu alloy with 24% prestrain (a) before and (b) after 12 h of aging at 550 °C. A magnetic field of 1.1 T was applied horizontally (along Q_x).

with 0% and 24% prestrain before and after aging at 550 °C for 12 h. The scattering intensities of the specimens with 8% prestrain are very similar to those for 24% prestrain. Before aging, the Fe-Cu alloy is fully solutionised and the SANS signal in Fig. 3 roughly follows a power-law behavior with a constant background for both the nuclear and the magnetic contributions (with a minor additional contribution of un-

known origin centered around 0.1 nm^{-1}). The additional scattering observed after aging is a result of the Cu precipitation. The data indicate that especially the magnetic scattering is strongly enhanced by aging. Without deformation, the additional contribution of the nuclear and magnetic scattering caused by aging has roughly the same Q dependence in the range $0.2 < Q < 2$ nm^{-1}, reflecting the formation of
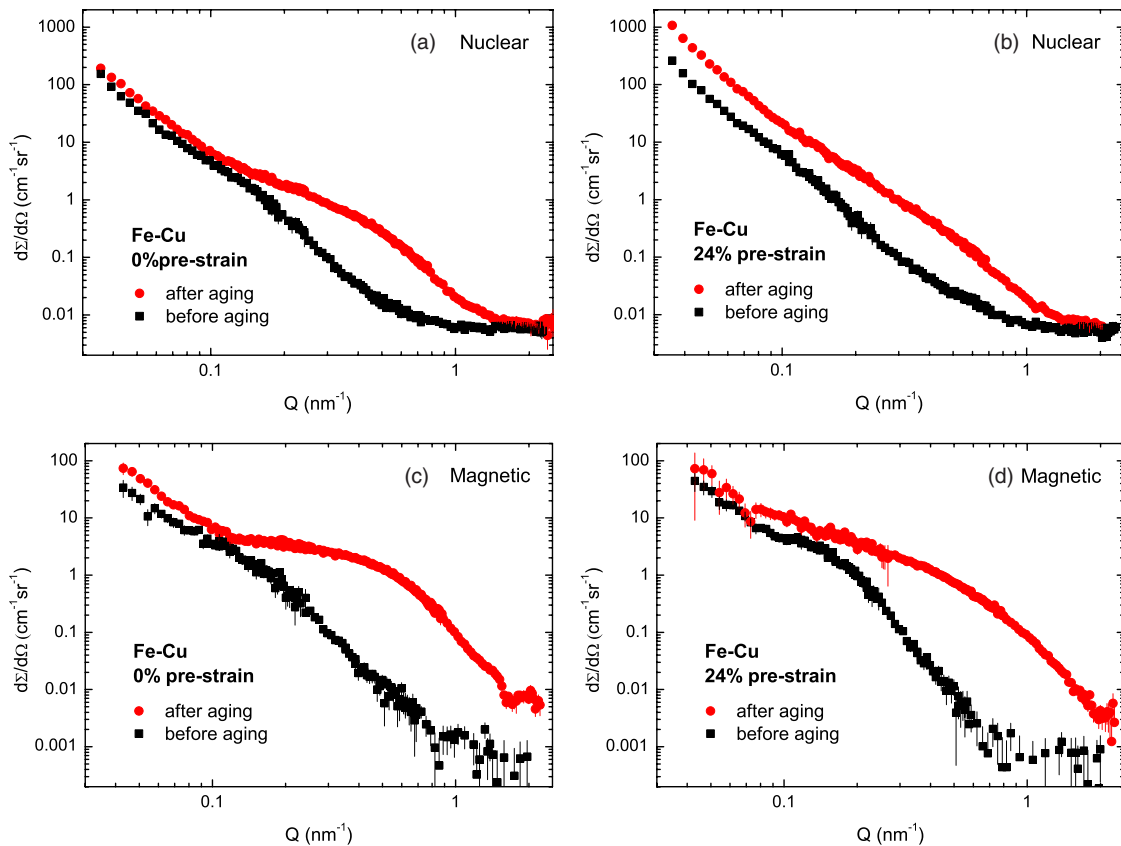

FIG. 3. (Color online) Nuclear and magnetic SANS components as a function of the wave-vector transfer Q for the Fe-Cu alloy with 0% and 24% prestrain measured at room temperature before and after aging at 550 °C for 12 h.
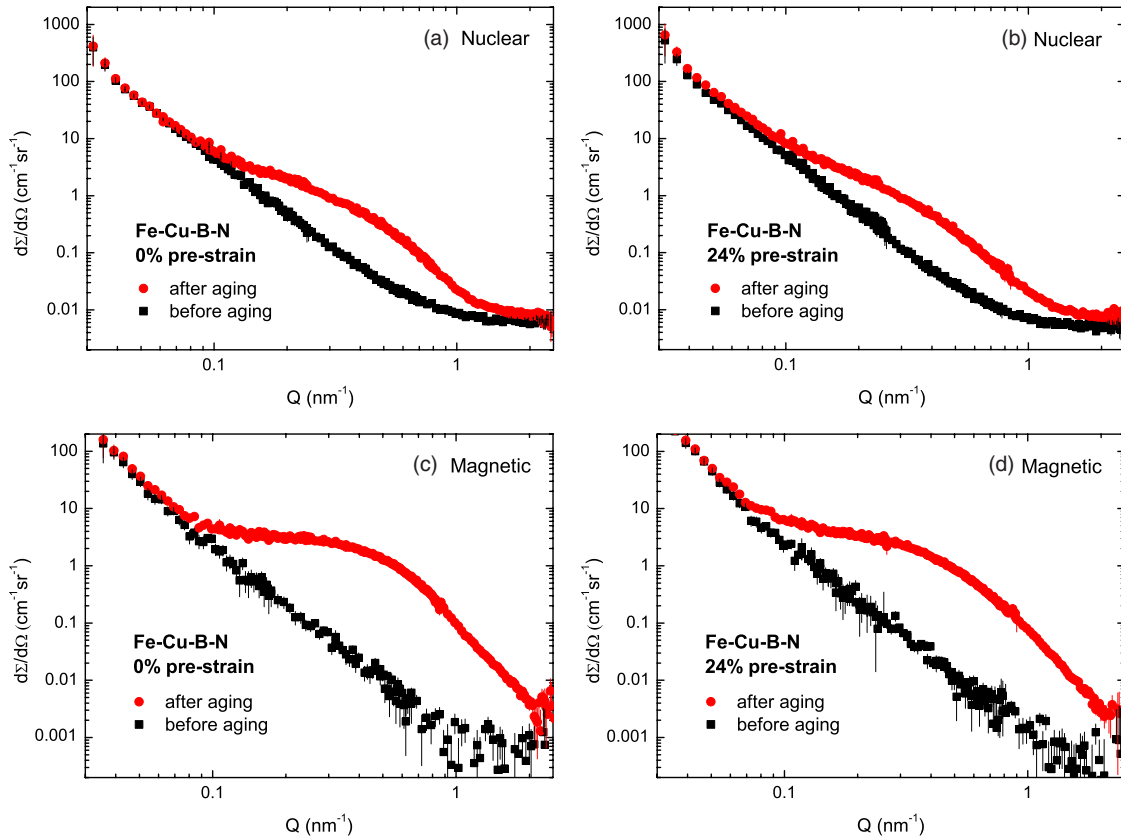
FIG. 4. (Color online) Nuclear and magnetic SANS components as a function of the wave-vector transfer Q for the Fe-Cu-B-N alloy with 0% and 24% prestrain measured at room temperature before and after aging at 550 °C for 12 h.

(spherical) nanoscale Cu precipitates. With 24% prestrain, a similar contribution is observed with a complementary increase in the power-law contribution for $Q < 0.1$ nm^{-1} in the nuclear scattering. This complementary nuclear contribution, observed for the deformed sample, reflects additional scattering from Cu precipitation at more extended objects (dislocations or interfaces).

For the Fe-Cu-B-N alloy (Fig. 4), the aging response of the SANS signal shows a similar increase in nuclear and magnetic scattering in the range $0.2 < Q < 2$ nm^{-1}, reflecting the formation of nanoscale Cu precipitates. In contrast, the

increase in nuclear scattering at low Q ($Q < 0.1$ nm^{-1}) is found to be much lower for the deformed Fe-Cu-B-N sample than for the deformed Fe-Cu sample after aging.

In order to monitor the time evolution during aging of the scattering from the nanoscale precipitates, we have evaluated the magnetic scattering by plotting $(d\Sigma/d\Omega)_{MAG}Q^2$ versus Q for the Fe-Cu and Fe-Cu-B-N alloys with 0%, 8%, and 24% prestrain. In Fig. 5 $(d\Sigma/d\Omega)_{MAG}Q^2$ versus Q is illustrated for the Fe-Cu alloys with 0% and 24% prestrain after subtraction of the initial scattering data from the as-quenched condition (note that the data for $Q < 0.2$ nm^{-1} have been suppressed).
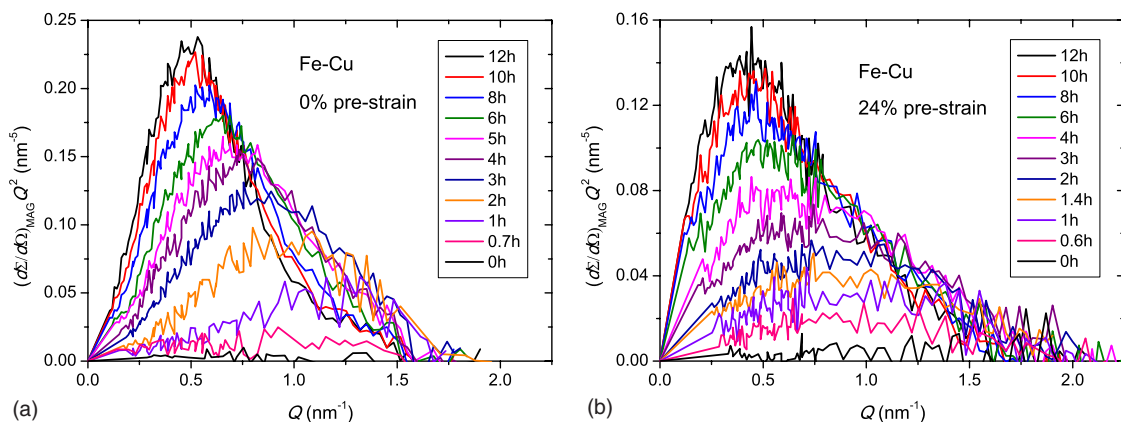

FIG. 5. (Color online) Time evolution of $(d\Sigma/d\Omega)_{MAG}Q^2$ as a function of Q for the Fe-Cu alloys with (a) 0% and (b) 24% prestrain during aging at 550 °C up to 12 h after subtraction of the initial scattering data for the homogenized condition before aging.

A progressive increase in $(d\Sigma/d\Omega)_{MAG}Q^2$ in the Q range 0.2–2 nm^{-1} is observed with a maximum around 0.5 nm^{-1} for all the samples. The maximum was found to decrease with increasing prestrain. The volume fraction f_V of nanosized Cu particles can be evaluated by integrating the $(d\Sigma/d\Omega)_{MAG}Q^2$ curve of magnetic scattering component.[31] From the area under the $(d\Sigma/d\Omega)Q^2$ curve for the magnetic (nuclear) scattering, the magnetic (nuclear) invariant Q_0 may be calculated,

$$Q_{0,i} = \int_0^\infty \left(\frac{d\Sigma}{d\Omega}\right)_i Q^2 dQ = 2\pi^2(\Delta\rho_i)^2 f_V(1-f_V), \quad (4)$$

where label i refers to the magnetic or nuclear SANS contribution, $\Delta\rho$ is the difference in the magnetic (nuclear) scattering length density of the matrix and the precipitate. The magnetic scattering length density amounts to $\rho_{MAG}=N_0 p_0 \mu$ for the ferromagnetic matrix, where N_0 is the number density of the magnetic moments, $p_0=2.699$ fm/μ_B is a constant and μ is the size of the magnetic moment. For the matrix, $N_0=8.49\times10^{28}$ m^{-3} and $\mu_{Fe}=1.718$ μ_B at $T=550$ °C, resulting in $\rho_{MAG}=3.94\times10^{14}$ m^{-2} ($\mu_{Fe}=2.225$ μ_B at room temperature).[32] For the nonmagnetic Cu precipitates, the magnetic scattering length density is zero. The corresponding nuclear contrast is $\Delta\rho_{NUC}=\rho_{Fe}-\rho_{Cu}\approx N_0^{Fe}b_c^{Fe}-N_0^{Cu}b_c^{Cu}$, where N_0 is the number density of atoms and b_c the coherent scattering length ($b_c^{Fe}=9.45\times10^{-15}$ m and $b_c^{Cu}=7.72\times10^{-15}$ m). The density of the copper precipitates depends on the stage in the structure evolution bcc$\rightarrow$9R$\rightarrow$3R$\rightarrow$fcc. At the initial stage of the transformation, coherent precipitates are formed ($N_0^{Cu}=N_0^{Fe}$), resulting in $\Delta\rho_{NUC}=1.47\times10^{14}$ m^{-2} ($\rho_{Fe}=8.02\times10^{14}$ m^{-2} and $\rho_{Cu}=6.55\times10^{14}$ m^{-2}). For the Fe-Cu-B-N alloy, nuclear and magnetic contrast is not significantly affected by the low concentration of added B and N. The same SANS measurements have also been performed on a high-purity Fe-B-N alloy (0.046 wt % B, 0.039 wt % N, and 0.015 wt % Ce). The time evolution of the SANS signal revealed only a weak strain-dependent aging response corresponding to precipitation at dislocations and interfaces. Potential reasons are: (1) the low solute concentrations of B an N and (2) the weak scattering contrast between the Fe matrix and the BN precipitates. For hexagonal BN the nuclear scattering length density amounts to $\rho_{BN}=7.75\times10^{14}$ m^{-2}, resulting in nuclear contrast of only $\Delta\rho_{NUC}=\rho_{Fe}-\rho_{BN}=0.27\times10^{14}$ m^{-2}. For the less stable cubic BN values of $\rho_{BN}=12.3\times10^{14}$ m^{-2} and $\Delta\rho_{NUC}=\rho_{Fe}-\rho_{BN}=-4.3\times10^{14}$ m^{-2} are found.

As the magnetic scattering from the copper precipitates is dominant $[(\Delta\rho_{MAG})^2>(\Delta\rho_{NUC})^2]$, we have used the magnetic component to estimate the phase fraction. For relatively small values, the volume fraction is estimated by $f_V\cong Q_{0,MAG}/2\pi^2(\Delta\rho_{MAG})^2$. In Figs. 6(a) and 6(b), the time evolution of the volume fraction of Cu precipitates, obtained by integrating the magnetic SANS component $(d\Sigma/d\Omega)_{MAG}Q^2$ up to the maximum Q value (2.5 nm^{-1}), is shown for the Fe-Cu and Fe-Cu-B-N alloys with 0%, 8%, and 24% prestrain.

For the Fe-Cu alloy [Fig. 6(a)], the precipitation in the initial aging stage (<1 h) is accelerated in the deformed samples with respect to the undeformed sample. This acceleration of the transformation kinetics can be explained by an increase in diffusion rate by fast pipe diffusion and an increase in potential nucleation sites. The dislocations generated by deformation are expected to act as nucleation sites for the copper precipitates by decreasing the activation energy for nucleation, most probably by a relief of strain energy. In the later stages (>2 h), the deformed Fe-Cu samples however approach a lower phase fraction of spherical Cu precipitates than the undeformed sample.

For the Fe-Cu-B-N alloy [Fig. 6(b)], a strongly enhanced Cu precipitation in the undeformed sample is observed at the start of the aging compared to the undeformed Fe-Cu sample. The deformed Fe-Cu-B-N samples, on the other hand, show a slightly faster precipitation kinetics compared to the deformed Fe-Cu sample with the same prestrain. The fraction transformed after 12 h of aging at 550 °C is nearly equal for the Fe-Cu alloys with and without added B and N. For both alloys, the fraction of nanoscale (spherical) precipitates reduces with the applied prestrain.

The equilibrium volume fraction of Cu precipitates is not expected to depend on the amount of prestrain. As shown in Figs. 6(a) and 6(b), the volume fraction of the spherical precipitates reached after 12 h of aging decreases however for increasing prestrain. This indicates that deformation either promotes Cu precipitation at dislocations and interfaces (resulting in additional scattering at lower Q values) or reduces the growth rate of the precipitates. It is interesting to note that additional room-temperature SANS experiments on samples that were aged for 96 h at 550 °C after applying a prestrain of 8% (samples of Ref. 30) indicated a volume fraction of the spherical precipitates of 0.57% for Fe-Cu and 0.59% for Fe-Cu-B-N.

In the Q range of 0.2–2 nm^{-1}, the nuclear SANS component shows the same time evolution as the magnetic SANS component with a lower intensity, reflecting the precipitation of nanoscale (spherical) Cu precipitates. As mentioned before, in the low-Q region (<0.2 nm^{-1}) an additional contribution to the nuclear scattering is observed that increases continuously with the aging time for the deformed samples. In order to monitor this additional contribution that reflects the precipitation of Cu along dislocations (and/or interfaces), we evaluated the time evolution of the nuclear scattering observed at low Q.

Experimentally, the nuclear scattered intensity $(d\Sigma/d\Omega)$ at low Q values (<0.2 nm^{-1}) is described by a power law of the form

$$(d\Sigma/d\Omega) = AQ^n + B, \quad (5)$$

where n is the exponent and A the coefficient of the power law while B corresponds to the background (due to incoherent scattering and diffuse coherent scattering). Within the experimental resolution, the exponent is found to be equal to $n=-4$ throughout the whole aging process for all the Fe-Cu and Fe-Cu-B-N samples with and without prestrain. For the homogenized sample, the Q^{-4} power-law behavior of the SANS signal at low Q originates from scattering of grain
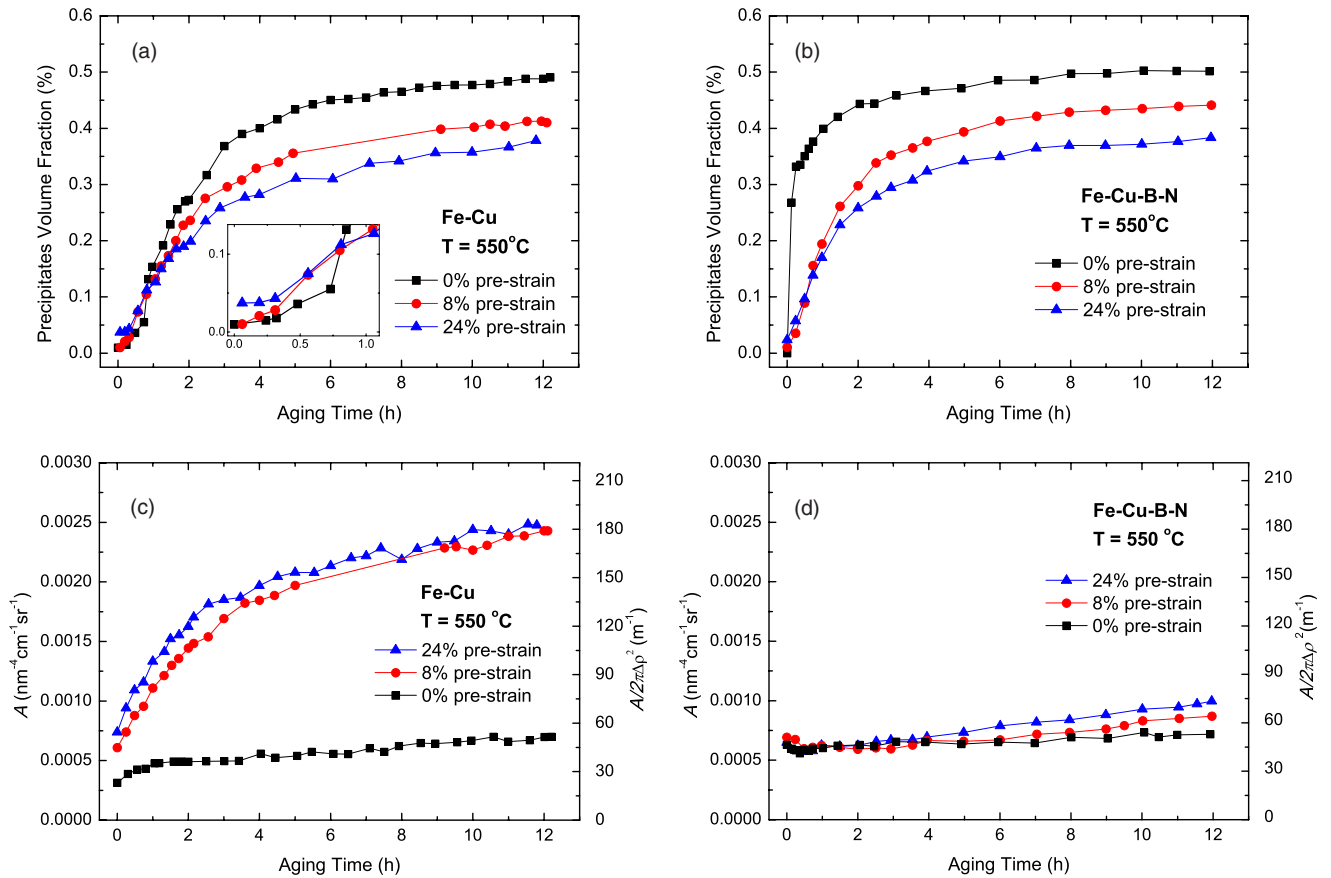
FIG. 6. (Color online) Time evolution of the volume fraction f_V for (a) the Fe-Cu alloy and (b) the Fe-Cu-B-N alloy with 0%, 8%, and 24% prestrain, derived from the magnetic SANS component shown during aging at 550 °C. For comparison, the time evolution of the coefficient A of the Q^{-4} power law is shown for (c) the Fe-Cu alloy and (d) the Fe-Cu-B-N alloy with 0%, 8%, and 24% prestrain, derived from nuclear SANS component around $Q=0.1$ nm^{-1} during aging at 550 °C. The inset in Fig. 6(a) shows the early aging stage up to 1.2 h.

boundaries. The increase in the size of the Q^{-4} power-law amplitude suggests Cu precipitation at dislocations (or interfaces).

Recently, the small-angle scattering from dislocations was analyzed in detail by Long and co-workers.[33,34] It was found that the strain fields associated with the dislocations give rise to a nuclear small-angle scattering signal in the form of a Q^{-2} power law for dislocation cores, Q^{-3} for dislocation dipoles and $Q^{-4}(1-\sigma^2 Q^{-2})$ for dislocation walls. In the low-Q range the scattering from dislocation walls will be dominant. For finite thickness walls with sharp boundaries ($\sigma=0$) the Q behavior becomes Q^{-4}. This prediction is in agreement with our experimental data. For magnetic scattering it is predicted[35] that the nuclear scattering term is multiplied by $(Q^2+Q_m^2)^{-2}$, where $1/Q_m$ is a characteristic magnetic scale for magnetostatic field variations. For $Q \ll Q_m$ the magnetic and nuclear scattering show the same Q^{-4} power law, as we found experimentally.

In Figs. 6(c) and 6(d), the time evolution of the coefficient A of the Q^{-4} power law during aging is shown for the Fe-Cu and Fe-Cu-B-N alloys with 0%, 8%, and 24% prestrain. For the Fe-Cu alloy [Fig. 6(c)], no significant increase in A is observed in the undeformed sample during aging while the predeformed samples show a strong increase with aging time. This strongly suggests that a significant fraction of the

nuclear scattering at low-Q values originates from a network of Cu atoms or clusters decorating the existing dislocations (or interfaces). The aging curves of A for the two deformed samples are close to each other but the most severely deformed sample with 24% prestrain exhibits the highest A value at all times. This means that the contribution from the network of Cu along dislocations (or interfaces) increases with the applied level of prestrain due to higher density of dislocations before aging. For the Fe-Cu-B-N alloy [Fig. 6(d)], only a very weak aging response is observed for A, with a slight increase for higher prestrains. The suppression of the aging response of A in the deformed Fe-Cu-B-N samples probably originates from a full decoration of the dislocations and interfaces by mobile N and/or B atoms before the less mobile Cu atoms have had the chance to precipitate at these sites.

It is important to note that the annealing response of the Q^{-4} power-law contribution in the nuclear scattering at low Q is considered to be related to the contrast in scattering length density of the Cu segregated at the dislocation walls and not due to a modification of the strain fields itself. This interpretation is confirmed by a comparison of the as-quenched samples with and without prestrain before aging. For these samples, which contain dislocations but no Cu precipitates, no significant enhancement in the low

Q (<0.2 nm^{-1}) part of the nuclear scattering is observed.

The increase in the coefficient A, caused by Cu precipitation at dislocations, is expected to scale with the contrast in scattering length density. For nuclear scattering, the scattering contrast $(\Delta\rho)^2$ originates from the difference in nuclear scattering length density of the alloy matrix ρ_m and the copper precipitate ρ_p. For comparison the value of $A/2\pi(\Delta\rho)^2$, which is proportional to the phase fraction of Cu precipitation at dislocations, is also shown in Fig. 6.

The increase in coefficient A for increasing prestrain [Figs. 6(c) and 6(d)] shows an inverse correlation with the volume fraction of spherical precipitates [Figs. 6(a) and 6(b)]. For the Fe-Cu-B-N alloys the signal of the copper precipitation at dislocations is much weaker than for the Fe-Cu alloys. A possible cause for this may be a reduced scattering contrast $(\Delta\rho)^2$ when Cu precipitates in combination with B and/or N at dislocations and interfaces.

Now that we have established the main contributions to the SANS signal, we can analyze the time evolution of the precipitate size distribution in detail. As discussed above, the neutron scattering from a ferromagnetic material (iron-based alloy) containing nonmagnetic particles with a different chemical composition (Cu-rich precipitates) generally contains both magnetic scattering and nuclear scattering components. The magnetic scattering originates from a difference in magnetization and the nuclear scattering from a difference in chemical composition. By applying a strong magnetic field to the specimen, these two components could be separated.[15,16] For a dilute system of particles embedded in a homogeneous matrix, the macroscopic differential scattering cross section ($d\Sigma/d\Omega$) characterizes the scattering power by[16,36]

$$\left(\frac{d\Sigma}{d\Omega}\right) = (\Delta\rho)^2 \int D_N(R)V(R)^2|F(Q,R)|^2 dR, \qquad (6)$$

where $\Delta\rho = \rho_p - \rho_m$ is the difference in the scattering length density of the precipitate ρ_p and the matrix ρ_m. The strength of the magnetic (nuclear) scattering is directly proportional to the magnetic (nuclear) contrast $(\Delta\rho)^2$. For spherical precipitates with a radius R, the particle volume is $V(R)=4\pi R^3/3$ and the form factor is $F(Q,R) = 3[\sin(QR)-(QR)\cos(QR)]/(QR)^3$. $D_N(R)$ is the size distribution function for the number of precipitates per unit volume. This number distribution $D_N(R)$ is directly related to the volume distribution $D_V(R)=V(R)D_N(R)$. Integration of $D_N(R)$ gives the number of precipitates per unit volume N_p while integration of $D_V(R)$ results in the volume phase fraction of the precipitates f_V.

In order to relate the scattering curves of the SANS experiments to the size distribution of the precipitates, some model assumptions have to be made. From previous TEM observations,[28] we know that the spherical Cu precipitates approximately show a log-normal size distribution $D_N(R)$ which is described by

$$D_N(R) = \frac{N_P}{R\sigma\sqrt{2\pi}}\exp\left\{-\frac{[\ln(R)-\ln(R_m)]^2}{2\sigma^2}\right\}, \qquad (7)$$

where N_P is the number density of precipitates, R_m is the median radius, and σ the standard deviation of the size distribution.

Figure 7 shows the log-normal volume distribution $D_V(=D_N V)$ of spherical Cu precipitates with precipitate radius R as a function of the aging time for the Fe-Cu and Fe-Cu-B-N alloys with 0%, 8%, and 24% prestrain. The particle size distributions were obtained by a fit of the magnetic SANS component with a log-normal distribution using the SASFIT program.[37] For short aging times (<1 h), the peak height of the volume distribution increases with the aging time without changing the peak position, indicating that nucleation is the dominant process in the very early aging stage. For longer aging times, the volume distribution of the Cu precipitates broadens, the peak height reduces and the peak position increases with aging time, suggesting that the growth of precipitates is the dominant process.

In Fig. 8, the time evolution of the median radius R_m and the number density N_P of the nanoscale precipitates is shown for the Fe-Cu and Fe-Cu-B-N alloys with 0%, 8%, and 24% prestrain during aging. The values of R_m and N_p follow directly from the fit [N_p is obtained by integration of the number distribution $D_N(R)$]. The mean radius R_m of spherical precipitates [Figs. 8(a) and 8(b)] initially increases roughly linearly with time under the influence of continuous nucleation and growth of the precipitates. In the later stages, the growth of the spherical precipitates closely follows a power law of the form $R_m = ct^{1/3}$, with a growth constant c that decreases with increasing prestrain. This power-law behavior is representative for coarsening of nucleated precipitates.[44,38] The decrease in c, observed for increasing prestrain, is probably due to the competing precipitation at dislocations and interfaces, which reduces the potential growth of spherical precipitates within the matrix. The number density N_p [Figs. 8(c) and 8(d)] rises rapidly to a very high level in the nucleation stage and subsequently decreases gradually during aging. The corresponding interparticle distance $L_p \propto 1/N_p^{1/3}$, on the other hand, gradually becomes larger for increasing aging time. This indicates that the growth of larger particles occurs at the expense of smaller particles.

C. Transmission electron microscopy

As shown in Fig. 9(a), for the undeformed Fe-Cu sample a limited number of larger Cu particles and few dislocations are observed in the TEM bright-field images after aging at 550 °C for 12 h. In Figs. 9(b) and 9(c), the TEM bright-field images are shown for the Fe-Cu sample with 8% prestrain after aging at 550 °C for 12 h. Copper precipitation is found as isolated particles within the matrix, as particles at pre-existing dislocations and as a Cu decorated network of dislocations and/or interfaces. The existence of twinned 9R particles (with a diameter of 6 nm) was confirmed in the studied Fe-Cu alloy by HREM [see Fig. 9(e)].

For the deformed Fe-Cu alloy, the Cu particles are preferentially formed on dislocations. Only a few particles are found to be larger than 30 nm in diameter and therefore, judged on their size, may have transformed to the equilibrium fcc lattice structure.

From traditional TEM images, only the Cu particles with a diameter bigger than 5 nm (critical size for the bcc→9R transition) are distinguishable. Because the smaller particles
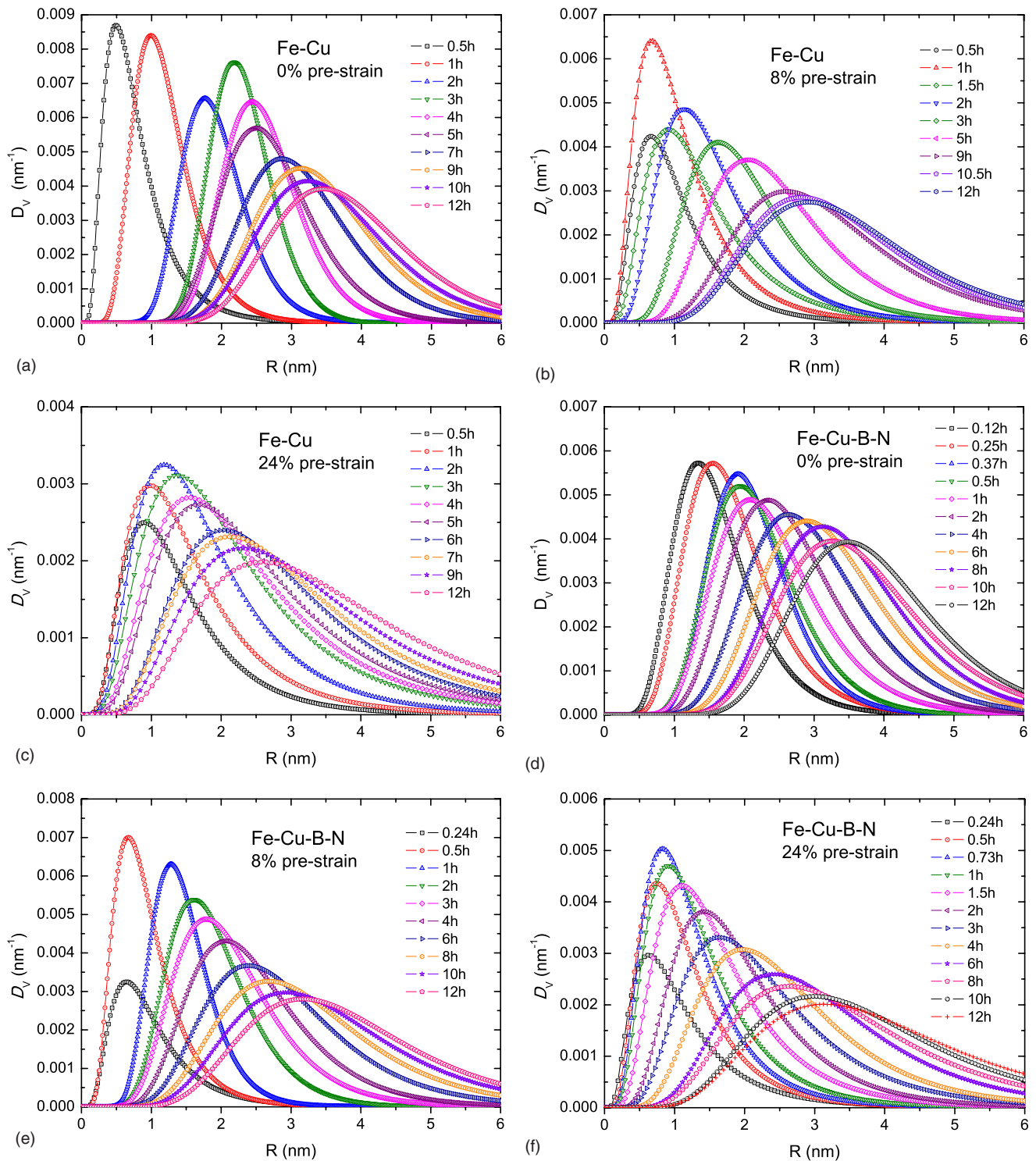
FIG. 7. (Color online) Volume distribution D_V of spherical Cu precipitates in (a)–(c) the Fe-Cu alloy and (d)–(f) the Fe-Cu-B-N alloy with 0%, 8%, and 24% prestrain during aging at 550 °C. D_V is derived from a fit of the time-resolved magnetic SANS data (see text).

are coherent with the matrix (with the same bcc crystal structure) and the difference of mass density between Cu and Fe is low, the contrast of these smallest particles is poor.

Comparing Figs. 9(a) and 9(b) to Fig. 9(c), it can be seen that there are more distinguishable precipitates in the 8% prestrained sample than in the undeformed sample. Moreover, the distinguishable Cu particles are predominantly con-

nected to heterogeneously distributed residual dislocations. In between the precipitates, dislocation-free regions are observed, where larger particles do not exist.

In Fig. 9(d), a TEM bright-field image for the 8% deformed Fe-Cu-B-N sample with 12 h aging at 550 °C is shown. Again, spherical Cu precipitates and dislocations are observed. However, compared to the Fe-Cu sample, fewer
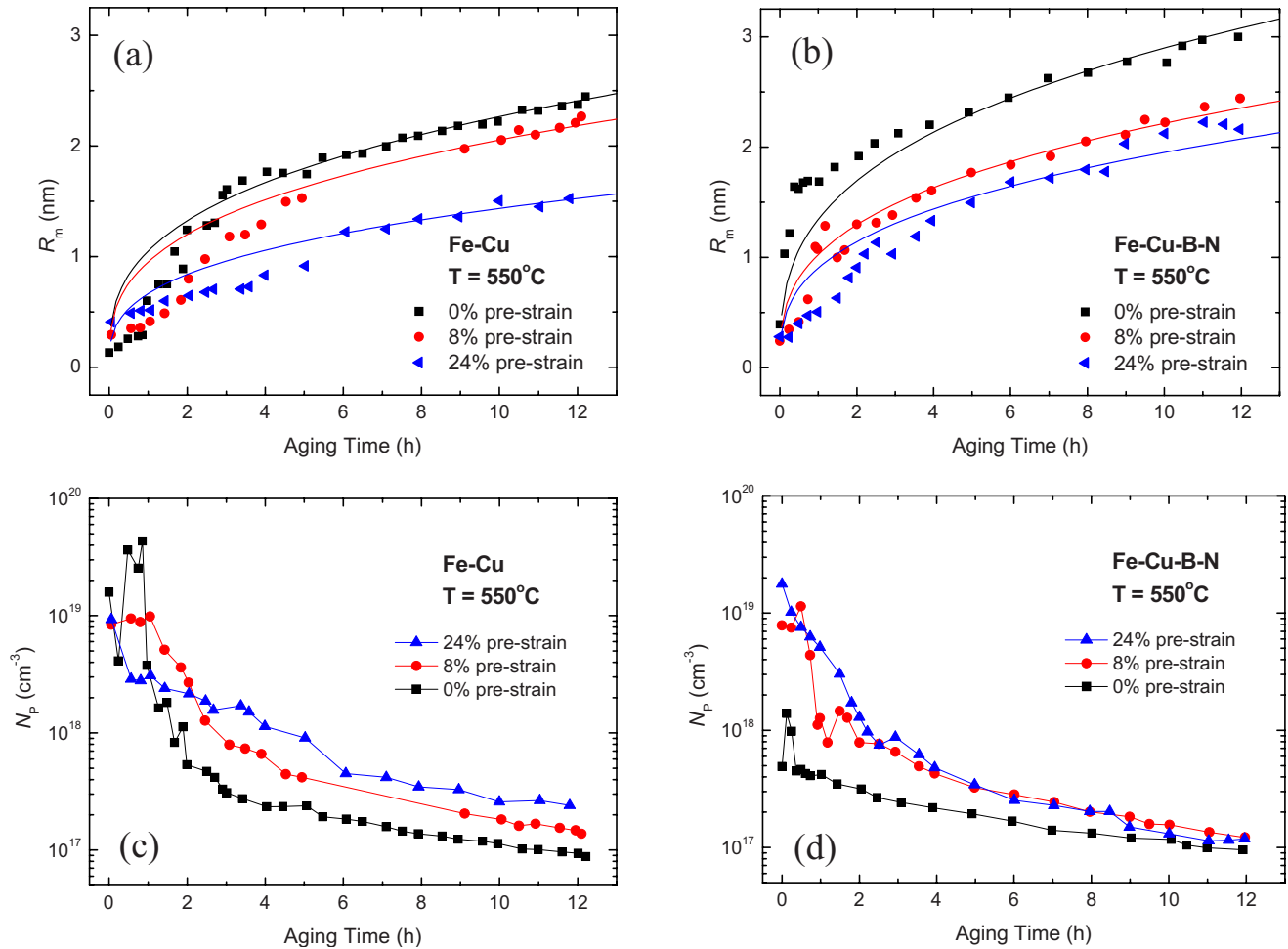
FIG. 8. (Color online) Time evolution of the median radius R_m and the number density N_P of spherical Cu precipitates in the Fe-Cu alloy and the Fe-Cu-B-N alloy with 0%, 8%, and 24% prestrain, derived from the magnetic SANS component during aging at 550 °C (see text).

copper precipitates are connected to the dislocations (or interfaces) and more are observed isolated in the matrix.

IV. DISCUSSION

A. Precipitation kinetics

The precipitation kinetics for Cu segregation in the homogenized Fe-Cu alloys shown in Fig. 7 is controlled by three different processes: (i) nucleation, (ii) growth and (iii) coarsening.[13] In the early-stage precipitation, Cu precipitates nucleate and subsequently grow in the homogenized matrix. As the phase fraction of precipitated Cu is small in the early stages, the homogenized matrix shows a high supersaturation of solute Cu. The growth of nucleated Cu precipitates initially shows no interaction with other precipitates. In this case the growth is described by the Zener model,[40] which predicts that the particle radius scales as $R \propto t^{1/2}$. When a significant phase fraction of Cu precipitates has formed then nucleation stops as the supersaturation of solute Cu is significantly lowered. At this stage the growth of individual precipitates becomes strongly correlated and is controlled by a coarsening process where the larger precipitates grow at the expense of the smaller precipitates that disappear.

Since dislocations act as fast pipe-diffusion paths and as heterogeneous nucleation sites, the precipitation kinetics is strongly affected by the dislocation structure. It has been found that dislocations are arranged in ordered patterns, consisting of dislocation cells and dislocation-free regions, during plastic deformation of Fe-Cu alloys[41] and pure copper.[42] The Cu particles located at dislocations and at the dislocation network, observed in Figs. 9(b) and 9(c) clearly signal the close interaction of Cu precipitation and dislocations during aging. The dislocation structure will generally vary with the deformation mode, strain level, and strain rate.[41,43,39]

In the early-stage precipitation regime (<4 h) copper precipitation at dislocations is strongly promoted by the prestrain in the Fe-Cu alloy. When N and/or B are added to the alloy, we see that the precipitation of copper at dislocations is largely suppressed. This is probably caused by the fast diffusion of mobile N and/or B to dislocations. A saturation with N and/or B effectively blocks Cu precipitation at dislocations. It is remarkable that the undeformed Fe-Cu-B-N sample has the fastest Cu precipitation kinetics of all the Fe-Cu and Fe-Cu-B-N samples. A possible explanation is that the nucleation barrier for copper precipitation in the matrix is lowered by the solute N and/or B. In the prestrained samples, a significant part of the solute N and/or B may have
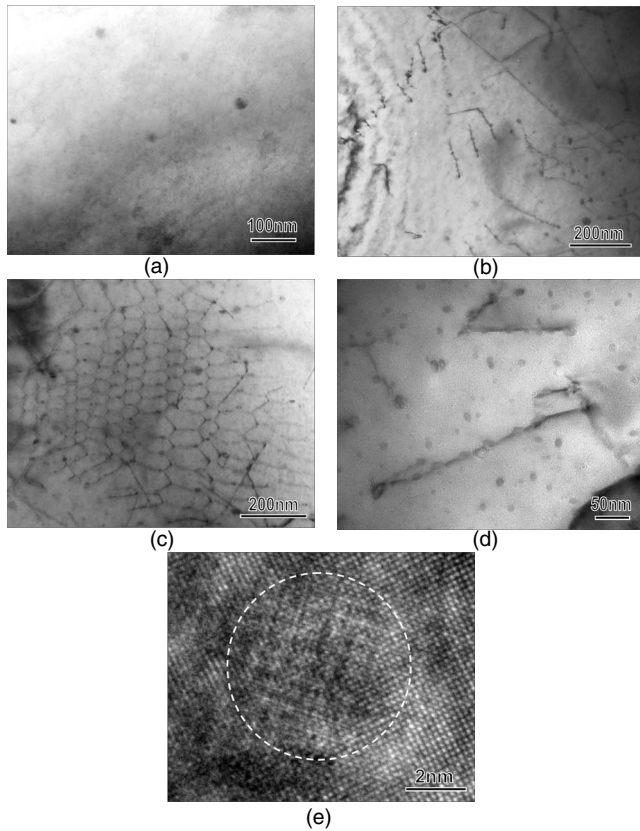
FIG. 9. TEM images of (a) the undeformed Fe-Cu alloy and (b) and (c) the Fe-Cu alloy with 8% prestrain and (d) the Fe-Cu-B-N alloy with 8% prestrain after aging at 550 °C for 12 h. In the undeformed sample (a) randomly distributed spherical Cu precipitates are observed. In the deformed samples (b)–(d) the dislocations are decorated with Cu precipitates. The Fe-Cu alloy with 8% prestrain (c) shows a network composed of dislocations and precipitates. In (e) the existence of twinned 9R particles in the Fe-Cu alloy was confirmed by high resolution electron microscopy (HREM).

preferentially segregated at dislocations, reducing the nucleation rate of Cu precipitates within the matrix.

In the later stages of aging (>4 h), the Cu concentration in the matrix is considerably reduced and the size evolution of the spherical nanoscale Cu precipitates is controlled by a coarsening of the formed precipitates. The growth of the precipitates during further aging is then described by the Lifshitz-Slyozov-Wagner (LSW) theory[44,38]

$$R_\mathrm{m}^3 = Kt, \qquad (8)$$

where R_m is the average radius of the precipitate. The deviations from the R^3 law, observed in the initial aging stage, originate from the simultaneous nucleation and growth processes. The LSW theory for coarsening with volume diffusion control for small volume fractions of spherical particles predicts the proportionality constant is given by

$$K = \frac{8D\Gamma C_\infty \Omega^2}{9kT} \propto \frac{C_\infty}{T}\exp(-Q/kT), \qquad (9)$$

where $D = 1.6 \times 10^{-18}$ m^2/s is the bulk diffusion coefficient of Cu in α-Fe at 550 °C,[45] $\Gamma = 0.58$ J/m^2 is the interfacial

energy between Cu and Fe,[46] $C_\infty = 0.18$ at. % the solubility limit of Cu in Fe at 550 °C,[47] $\Omega = 1.18 \times 10^{-29}$ m^3/atom the atomic volume of solute in the dispersed phase, Q the activation energy of bulk Cu diffusion in Fe, k Boltzmann's constant, and T temperature. For the Fe-Cu alloy, the experimental value of the proportionality constant at 550 °C amounts to $K_{0\%} = 2.9 \times 10^{-31}$ m^3/s for the undeformed sample, which is significantly lower than the value of $K = 9.4 \times 10^{-31}$ m^3/s reported by Monzen and co-workers at a temperature of 650 °C.[46] The experimental values of $K_{8\%} = 2.6 \times 10^{-31}$ m^3/s for 8% prestrain and $K_{24\%} = 1.9 \times 10^{-31}$ m^3/s for 24% prestrain indicate that the growth rates for spherical Cu particles in the matrix decreases with increasing dislocation densities. The lower growth rates of the predeformed samples may be related to the reduced Cu concentration in dislocation-free regions due to the segregation of Cu at dislocations.

When we compare the volume fraction of Cu occupied by the spherical nanoscale precipitates after 12 h aging at 550 °C, we see that about half of the nominal copper concentration has formed precipitates for both the Fe-Cu and Fe-Cu-B-N samples. With increasing prestrain, a slight decrease in the precipitated volume fraction is observed for both alloys. In SAXS measurements on deformed Fe-Cu alloys,[28] it was reported that the volume fraction of Cu precipitates increases faster in the predeformed sample than in the undeformed sample but saturates at the same value for long aging times up to 300 h at 500 °C. They claimed that in peak-hardness condition the Fe-Cu alloy has not reach a complete precipitation and the volume fraction of precipitates reaches about 48% and 52% of equilibrium value for the undeformed and deformed samples.

B. Structure evolution of the precipitates

Experimentally, it was found that in binary Fe-Cu alloys the structure evolution of Cu precipitates follows the sequence bcc$\rightarrow$9R$\rightarrow$3R$\rightarrow$fcc.[7,48] It is believed that the structure changes in the Cu precipitates is triggered by a critical size and driven by minimizing the interfacial strain energy. The volume strain energy within the Cu precipitate is relatively weak because the difference in atomic radii of Fe and Cu is small (3%). When the nucleated coherent bcc clusters grow in size they transform into the 9R structure beyond a critical size of 4–6 nm in diameter, followed by the transformation from the 9R structure to the 3R or fcc structure at a critical size of 15–17 nm in diameter.

Using the fitted particle size distributions for the spherical nanoscale Cu precipitates of Fig. 7, we can now, based on the reported critical sizes, estimate what fraction of the formed precipitates has a bcc structure, 9R structure or 3R/fcc structure. The volume fraction is now directly obtained by integration of the volume distribution $D_\mathrm{V}(R)$ while the number fraction is obtained by integration of the number distribution $D_\mathrm{N}(R)$. Figure 10 shows the estimated evolution of the relative volume and number fraction of the Cu precipitates in the Fe-Cu and Fe-Cu-B-N alloys during aging at 550 °C. For this evaluation, we have used a critical radius of $R_{\mathrm{bcc}\rightarrow 9R} = 2.5$ nm for the transition from the bcc structure to
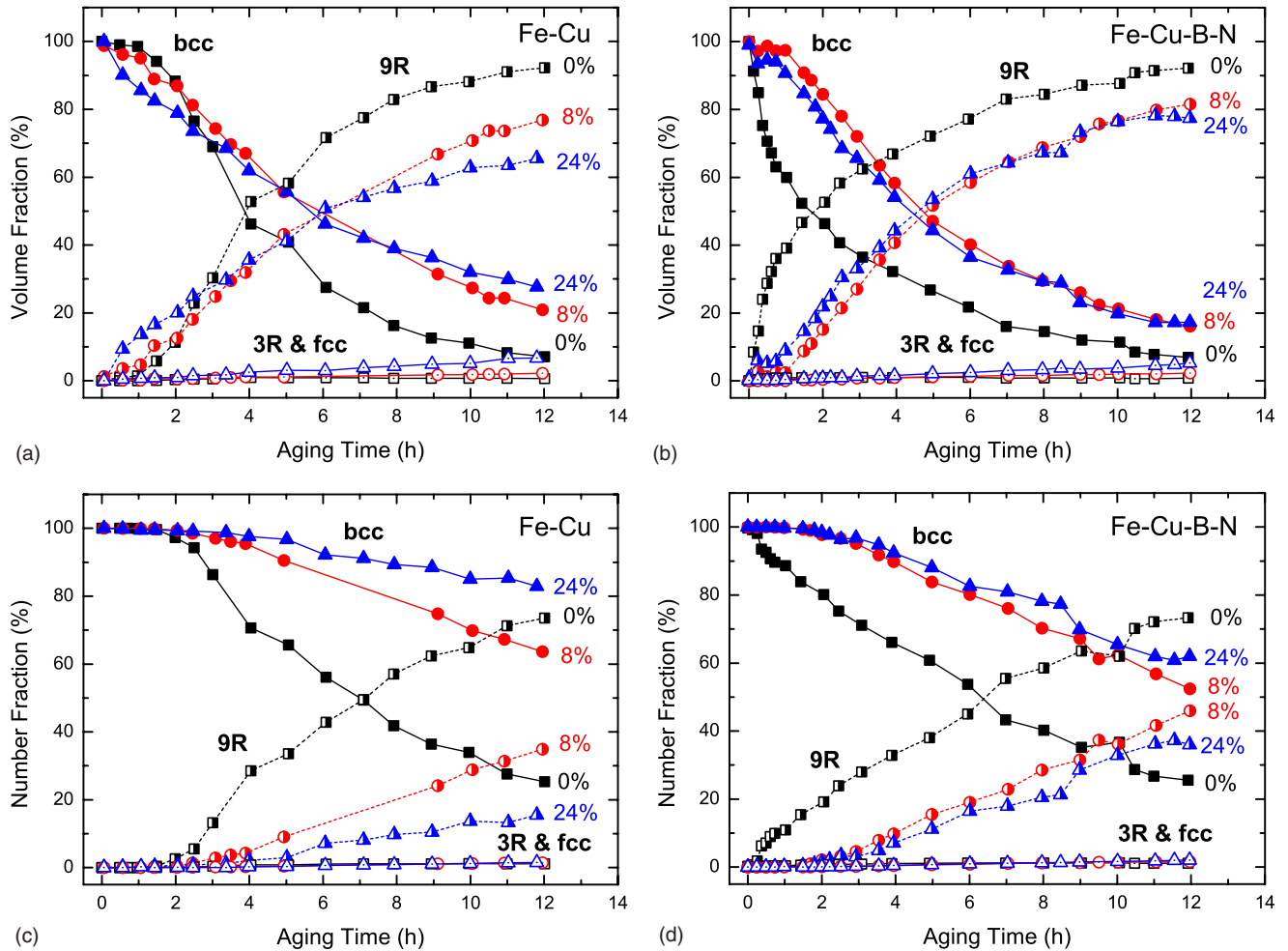
FIG. 10. (Color online) Time evolution of the fractional contributions of Cu precipitates with a bcc (solid), 9R (half solid), and 3R and fcc (open) structure for the Fe-Cu alloys with 0% (square), 8% (circle), and 24% (triangle) prestrain during aging at 550 °C. The fractional contributions are obtained from the experimental particle size distributions.

the 9R structure and a critical radius of $R_{9R\rightarrow3R/fcc}=8$ nm for the transition from the 9R structure to the 3R or fcc structure. In this evaluation we have assumed that the structural changes are purely determined by the size of the precipitate as the structure itself is not probed in the SANS measurements.

For the Fe-Cu alloy, prestrain accelerates the transition from the coherent bcc structure to the incoherent 9R while for the Fe-Cu-B-N alloy prestrain delays the formation of the 9R structure. Within 12 h of aging at 550 °C, only a minor fraction of the copper precipitates have reached a size corresponding to the 3R or fcc structure. The prestrain slightly promotes the 9R→3R or fcc transformation for both the alloys. It is noted that in peak-hardness condition, which was reached after an aging time of about 6 h for Fe-Cu and about 4 h for Fe-Cu-B-N, the undeformed samples show a dominant phase fraction with the 9R structure, while for the deformed samples equal phase fractions of about 50% are found for the bcc and 9R structure. For the Fe-Cu sample with 8% prestrain, a significant fraction of semicoherent precipitates with a 9R structure forms after about 1 h. This is consistent with earlier positron annihilation spectroscopy measurements on the same material.[30]

C. Self-healing of defects

In previous studies on austenitic stainless steels, it was found that the addition of B with N and Cu both lead to a significant increase in the creep lifetime at high temperatures.[2,3] The improved creep lifetime was ascribed to a self-healing of nucleated creep cavities by the formation of BN and/or Cu precipitates. Here we have systematically studied the aging behavior of prestrained high-purity Fe-Cu and Fe-Cu-B-N alloys by time-resolved SANS measurements at a temperature of 550 °C. From the observed precipitation kinetics, we have evaluated the influence of prestrain and added B and N on the precipitation kinetics of Cu. For the Fe-Cu alloy, Cu has a strong tendency to segregate at open volume defects such as dislocations, which is expected to be very beneficial for self-healing of creep cavities. Simultaneously, copper is also precipitating within the matrix which leads to a precipitation strengthening of the alloy (until peak aging is reached). For the Fe-Cu-B-N alloy, the addition of boron and nitrogen accelerates the formation of spherical Cu precipitates within the matrix, but strongly reduces the Cu precipitation along dislocations in the deformed samples. Both effects are probably caused by a fast segregation of the mobile B and N atoms along dislocations, pre-

venting Cu precipitation along these dislocations, but promoting the nucleation of nanoscale Cu precipitates in dislocation-free regions. The enhanced nucleation of nanoscale Cu precipitates is either due to the effect of remnant B and N or the lower loss in Cu for the dislocation-free regions, compared to the Fe-Cu alloy with the same prestrain. One therefore expects that in Fe-Cu-B-N alloys self-healing of small defects will initially take place by the formation of BN precipitates, and may be assisted by copper precipitation when larger creep cavities are formed.

V. CONCLUSIONS

We have performed time-resolved SANS measurements during isothermal aging at a temperature of 550 °C in order to study the influence of tensile deformation on the precipitation kinetics of copper in a high-purity Fe-Cu and Fe-Cu-B-N alloys. The time evolution of the precipitate size distribution was monitored at high temperatures for copper solutionised samples with 0%, 8%, and 24% strain applied by prior tensile deformation. Complementary TEM measurements were performed on the aged samples to characterize the formed precipitates. The mechanical behavior was evaluated by hardness tests as a function of aging time. The main conclusions derived from these experiments are: (1) the SANS signal of the Fe-Cu and Fe-Cu-B-N alloys indicate that the precipitation of copper occurs in the form of (a) spherical nanoscale precipitates within the grains and (b) decoration of dislocations and/or interfaces. Both contributions were monitored independently as a function of aging time.

(2) For the Fe-Cu alloy, the presence of dislocations resulting from the prestrain promotes the nucleation of spherical nanoscale precipitates whereas the growth seems to be retarded. The precipitation of Cu along dislocations is strongly promoted by increasing levels of prestrain.

(3) For the Fe-Cu-B-N alloy, the addition of boron and nitrogen accelerates the formation of spherical nanoscale Cu precipitates and strongly reduces the Cu precipitation along dislocations in deformed samples. Both effects are probably caused by a fast segregation of the mobile B and N atoms along dislocations, preventing Cu precipitation along these dislocations, but promoting the nucleation of nanoscale Cu precipitates. One therefore expects that in Fe-Cu-B-N alloys self-healing of small defects will initially take place by the formation of BN precipitates.

(4) The experimental time evolution of the particle size distribution for spherical nanoscale copper precipitates gives a direct estimate of the fraction of copper precipitates with a coherent bcc structure, a 3R structure, and a 9R or fcc structure. The transition from coherent to partially incoherent Cu clusters is in good agreement with recent positron annihilation spectroscopy results.[30]

*Corresponding author. FAX: +31(0)152788303; hsm3152k@yahoo.com.cn

[1] R. N. Lumley, A. J. Morton, and I. J. Polmear, Acta Mater. **50**, 3597 (2002).

[2] K. Laha, J. Kyono, S. Kishimoto, and N. Shinya, Scr. Mater. **52**, 675 (2005).

[3] K. Laha, J. Kyono, and N. Shinya, Scr. Mater. **56**, 915 (2007).

[4] *Self-Healing Materials: An Alternative Approach to 20 Centuries of Materials Science*, Springer Series in Materials Science Vol. 100, edited by S. van der Zwaag (Springer, Dordrecht, 2007).

[5] U. Dahmen, P. Ferguson, and K. H. Westmacott, Acta Metall. **32**, 803 (1984).

[6] P. J. Othen, M. L. Jenkins, G. D. W. Smith, and W. J. Phythian, Philos. Mag. Lett. **64**, 383 (1991).

[7] P. J. Othen, M. L. Jenkins, and G. D. W. Smith, Philos. Mag. A **70**, 1 (1994).

[8] R. Monzen, M. L. Jenkins, and A. P. Sutton, Philos. Mag. A **80**, 711 (2000).

[9] M. K. Miller, P. Pareige, and M. G. Burke, Mater. Charact. **44**, 235 (2000).

[10] P. Pareige, K. F. Russell, and M. K. Miller, Appl. Surf. Sci. **94-95**, 362 (1996).

[11] P. Pareige and M. K. Miller, Appl. Surf. Sci. **94-95**, 370 (1996).

[12] D. Isheim, M. S. Gagliano, M. E. Fine, and D. N. Seidman, Acta Mater. **54**, 841 (2006).

[13] R. Kampmann and R. Wagner, in *Atomic Transport and Defects in Metals by Neutron Scattering*, edited by C. Janot, W. Petry, D. Richter, and T. Springer (Springer-Verlag, Berlin, 1986), p. 73.

[14] G. M. Worrall, J. T. Buswell, C. A. English, M. G. Hetherington, and G. D. W. Smith, J. Nucl. Mater. **148**, 107 (1987).

[15] K. Osamura, H. Okuda, M. Takashima, K. Asano, and M. Furusaka, Mater. Trans., JIM **34**, 305 (1993).

[16] K. Osamura, H. Okuda, S. Ochiai, M. Takashima, K. Asano, M. Furusaka, K. Kishida, and F. Kurosawa, ISIJ Int. **34**, 359 (1994).

[17] Y. Nagai, M. Hasegawa, Z. Tang, A. Hempel, K. Yubuta, T. Shimamura, Y. Kawazoe, A. Kawai, and F. Kano, Phys. Rev. B **61**, 6574 (2000).

[18] Y. Nagai, T. Chiba, Z. Tang, T. Akahane, T. Kanai, M. Hasegawa, M. Takenaka, and E. Kuramoto, Phys. Rev. Lett. **87**, 176402 (2001).

[19] K. Sumiyama, Y. Yoshitake, and Y. Nakamura, Acta Metall. **33**, 1785 (1985).

[20] P. Asoka-Kumar, B. D. Wirth, P. A. Sterne, R. H. Howell, and G.

R. Odette, Philos. Mag. Lett. **82**, 609 (2002).

[21] J. J. Blackstock and G. J. Ackland, Philos. Mag. A **81**, 2127 (2001).

[22] Y. Le Bouar, Acta Mater. **49**, 2661 (2001).

[23] J.-H. Shim, Y. W. Cho, S. C. Kwon, W. W. Kim, and B. D. Wirth, Appl. Phys. Lett. **90**, 021906 (2007).

[24] E. Kozeschnik, Scr. Mater. **59**, 1018 (2008).

[25] M. Legros, G. Dehm, E. Arzt, and T. J. Balk, Science **319**, 1646 (2008).

[26] C. Zhang, M. Enomoto, T. Yamashita, and N. Sano, Metall. Mater. Trans. A **35**, 1263 (2004).

[27] K. Osamura, H. Okuda, K. Asano, M. Furusaka, K. Kishida, F. Kurosawa, and R. Uemori, ISIJ Int. **34**, 346 (1994).

[28] A. Deschamps, M. Militzer, and W. J. Poole, ISIJ Int. **41**, 196 (2001).

[29] A. Deschamps, M. Militzer, and W. J. Poole, ISIJ Int. **43**, 1826 (2003).

[30] S. M. He, N. H. van Dijk, H. Schut, E. R. Peekstok, and S. van der Zwaag, Phys. Rev. B **81**, 094103 (2010).

[31] A. Wiedenmann, in *Neutron Scattering from Magnetic Materials*, edited by T. Chatterji (Elsevier, Amsterdam, 2006), p. 473.

[32] A. S. Arrott and B. Heinrich, J. Appl. Phys. **52**, 2113 (1981).

[33] G. G. Long and L. E. Levine, Acta Crystallogr., Sect. A: Found. Crystallogr. **61**, 557 (2005).

[34] R. Thomson, L. E. Levine, and G. G. Long, Acta Crystallogr., Sect. A: Found. Crystallogr. **55**, 433 (1999).

[35] W. Schmatz, T. Springer, J. Schelten, and K. Ibel, J. Appl. Crystallogr. **7**, 96 (1974).

[36] N. H. van Dijk, W. G. Bouwman, S. E. Offerman, M. Th. Rekveldt, J. Sietsma, S. van der Zwaag, A. Bodin, and R. K. Heenan, Metall. Mater. Trans. A **33**, 1883 (2002).

[37] J. Kohlbrecher and I. Bressler, SASFIT: software package for fitting small-angle scattering curves, http://kur.web.psi.ch/sans1/SANSSoft/sasfit.html

[38] I. M. Lifshitz and V. V. Slyozov, J. Phys. Chem. Solids **19**, 35 (1961).

[39] C. Wagner, Z. Elektrochem. **65**, 581 (1961).

[40] C. Zener, J. Appl. Phys. **20**, 950 (1949).

[41] T. Ishizaki, T. Yoshiie, K. Sato, S. Yanagita, Q. Xu, M. Komatsu, and M. Kiritan, Mater. Sci. Eng., A **350**, 102 (2003).

[42] B. Jakobsen, H. F. Poulsen, U. Lienert, J. Almer, S. D. Shastri, H. O. Sørensen, C. Gundlach, and W. Pantleon, Science **312**, 889 (2006).

[43] K. Sato, M. Kai, K. Mitoma, Q. Xu, and T. Yoshiie, Phys. Status Solidi C **4**, 3559 (2007).

[44] D. Hughes, D. C. Chrzan, Q. Liu, and N. Hansen, Acta Mater. **45**, 105 (1997).

[45] M. Perez, M. Dumont, and D. Acevedo-Reyes, Acta Mater. **56**, 2119 (2008).

[46] R. Monzen, K. Takada, and C. Watanabe, ISIJ Int. **44**, 442 (2004).

[47] M. Perez, F. Perrard, V. Massardier, X. Kleber, A. Deschamps, H. De Monestrol, P. Pareige, and G. Covarel, Philos. Mag. **85**, 2197 (2005).

[48] E. Hornbogen, Acta Metall. **10**, 525 (1962).